Further studies on the evidence for a 17-keV neutrino in a ^{14}C-doped germanium detector

F.E. Wietfeldt,[1,2,*] E.B. Norman,[1] Y.D. Chan,[1] M.T.F. da Cruz,[1,3] A. García,[1,4] E.E. Haller,[5,6] W.L. Hansen,[5] M.M. Hindi,[1,7] R.-M. Larimer,[1] K.T. Lesko,[1] P.N. Luke,[5] R.G. Stokstad,[1] B. Sur,[1,†] and I. Žlimen[1,‡]

[1]*Nuclear Science Division, Lawrence Berkeley Laboratory, Berkeley, California 94720*

[2]*Physics Department, University of California, Berkeley, California 94720*

[3]*Physics Institute, University of São Paulo, São Paulo, Brazil*

[4]*Physics Department, University of Notre Dame, Notre Dame, Indiana 46556*

[5]*Engineering Division, Lawrence Berkeley Laboratory, Berkeley, California 94720*

[6]*Department of Materials Science and Mineral Engineering, University of California, Berkeley, California 94720*

[7]*Physics Department, Tennessee Technological University, Cookeville, Tennessee 38505*

(Received 15 September 1994; revised manuscript received 24 February 1995)

We have studied the beta spectrum of ^{14}C using a unique ^{14}C-doped germanium detector. In 1991 an initial report was made of a distortion in the spectrum that could be explained by the emission of a 17-keV neutrino in approximately 1% of the decays. Further tests have shown that the observed distortion was most likely caused by systematic effects related to the detector's active guard ring. A new measurement with a smaller data sample shows no sign of this distortion. In addition, we find the Q value of ^{14}C decay to be 155.95 ±0.07 (stat.) ±0.21 (sys.) keV, in disagreement with a previous precision measurement.

PACS number(s): 23.40.Bw, 14.60.Pq, 27.20.+n

I. INTRODUCTION

The allowed theoretical beta decay energy spectrum is given by

$$\frac{dN(E,m_\nu)}{dE} \propto F(Z,E)pE\,(Q-E)\left[(Q-E)^2-m_\nu^2\right]^{\frac{1}{2}}, \tag{1}$$

where p, E are the beta momentum and energy, Q is the total decay energy, $F(Z,E)$ accounts for final-state Coulomb effects, and m_ν is the electron neutrino mass which is assumed to be zero in the standard model. If neutrinos are massive particles, the neutrino mass eigenstates will in general be related to the weak interaction states by a unitary transformation:

$$|\nu_l\rangle = \sum_i U_{li}|\nu_i\rangle\ , \tag{2}$$

where ν_l are the weak states (l=e,μ,τ) and ν_i are the mass eigenstates (i=1,2,3). U is the leptonic mixing matrix, analogous to the Cabibbo-Kobayashi-Maskawa matrix found in the quark sector. Suppose the electron neutrino couples dominantly to two mass states with masses $m_1 \approx 0$ and $m_2 \gg m_1$. An observed nuclear beta decay spectrum will then consist of an incoherent superposition of the spectra corresponding to $m_\nu \approx 0$ and $m_\nu = m_2$ [1]:

$$\frac{dN(E)}{dE} = \cos^2\theta\frac{dN(E,0)}{dE} + \sin^2\theta\frac{dN(E,m_2)}{dE} \tag{3}$$

with $\cos\theta \approx |U_{e1}|$, $\sin\theta \approx |U_{e2}|$.

It is convenient to write (3) as the product of the massless neutrino spectrum and a massive neutrino shape factor $S(E)$,

$$\frac{dN(E)}{dE} \propto \frac{dN(E,0)}{dE}S(E) \tag{4}$$

with

$$S(E) = 1+\tan^2\theta\left[1-\frac{m_2^2}{(Q-E)^2}\right]^{\frac{1}{2}} \text{ for } E \le Q-m_2,$$
$$= 1 \text{ for } E > Q-m_2. \tag{5}$$

For $E > Q-m_2$ the heavy neutrino is energetically forbidden and the spectrum is identical to the massless neutrino spectrum. There is a kink (slope discontinuity) at $E = Q-m_2$ and below that point the relative amplitude rises to $1+\tan^2\theta$. The values of m_2 and θ will be the same in all beta spectra having $Q > m_2$.

In 1985 Simpson observed a distortion in the tritium beta decay spectrum that he interpreted to be the result of a massive neutrino admixture with $m_2 \approx 17$ keV and $\sin^2\theta \approx 1$–3% [2]. The experiment consisted of a Si(Li) detector in which tritium had been implanted to a depth sufficient to stop all the tritium betas and bremsstrahlung photons, yielding a fully calorimetric beta spectrum. During the next 2 years, magnetic spectrometer mea-

*Present address: NIST, Gaithersburg, MD 20899.

†Present address: Chalk River Laboratories, Chalk River, Ontario, Canada K0J1J0

‡On leave from Rugjer Bošković Institute, Zagreb, Croatia.

surements of ^{35}S [3–5] and ^{63}Ni [6] beta spectra were conducted and Simpson's result was not confirmed. Solid-state detector experiments using external ^{35}S [7,8] and ^{125}I [9] sources also failed to observe the 17-keV neutrino. Simpson and Hime responded in 1989 with a pair of papers that described new results from a tritium-implanted germanium detector and a solid-state, external-source ^{35}S measurement, both showing strong evidence for a 1% admixture of a 17-keV neutrino [10]. They also reviewed and criticized all of the negative experiments.

In 1991 our group at Berkeley reported a preliminary result from the measurement of a ^{14}C-doped germanium detector [11]. A spectral distortion was seen near the end point that was consistent with the emission of a neutrino of mass 17 ± 2 keV and $\sin^2\theta = 1.4 \pm 0.5\%$. As in the tritium experiments, the source was contained within the active volume of the detector, eliminating most scattering and energy loss effects that complicate the detector response. The activity was introduced when the detector crystal was grown, rather than implanted after growth (which can cause radiation damage to the crystal). The decay energy of ^{14}C (156 keV) is much higher than that of tritium (18.6 keV), so atomic and environmental effects are much less important. In the same year, new results supporting the 17-keV neutrino were announced by groups studying ^{35}S and ^{63}Ni beta decay [12] and ^{71}Ge electron capture decay [13].

The experimental controversy over the 17-keV neutrino caused considerable excitement in nuclear and particle physics. This excitement was short-lived; second-generation experiments in 1992–94, using improved detection and analysis techniques, all reported negative results [14–22] and the 17-keV neutrino was convincingly ruled out. However, it remains interesting and important to study the positive experiments and try to understand the cause(s) of their erroneous results.

The purpose of this paper is to describe in detail the ^{14}C-doped germanium detector experiment, to discuss the various tests that we performed to study anomalies in its behavior, and to offer an explanation for the distortion that was originally observed.

II. THE DETECTOR

The beta decay of ^{14}C to ^{14}N is an allowed ground-state to ground-state transition with $Q_\beta \approx 156$ keV and a half-life of 5730 years [23]. By introducing a radioactive carbon sample into the germanium melt prior to crystal growth, a ^{14}C-doped germanium detector can be produced with no radiation damage. The maximum range of a 150-keV beta in germanium is 84 μm [24] so, with a sufficiently large detector, the efficiency is nearly 100% and a fully calorimetric measurement of the ^{14}C beta spectrum can be made. This seemed an excellent way to test Simpson's claim of a 17-keV neutrino; the kink would appear at 139 keV where the energy calibration is straightforward and atomic effects are negligible.

Fortuitously, a number of such ^{14}C-doped germanium detectors were constructed in 1982 in order to study the solubility of carbon in germanium [25]. Although they are found in the same periodic group, carbon and germanium are metallurgically immiscible. To make these detectors, a mixture of ^{14}C-methane (8.8%) and ^{12}C-methane (91.2%) was introduced into a silica reaction chamber which contained a silica crucible held at 1050°C. This temperature was high enough to pyrolyze the methane and coat all surfaces inside the chamber with free carbon. Two crucibles were coated in this way, and several germanium crystals were then grown in these crucibles. Some of the crystals were made into radiation detectors, and by integrating the resulting beta spectra, the total carbon concentrations were obtained, ranging from 1.0×10^{14} to 4.5×10^{15} cm^{-3}. Autoradiographs were taken by sandwiching thin slices of the crystals between sheets of x-ray film and allowing the film to be exposed to the ^{14}C beta activity for a period of 3 months. This revealed that much of the carbon was concentrated into clusters of varying size, although the absolute sizes and numbers of clusters could not be quantitatively determined.

One of the crystals was melted and regrown in a bare crucible. An autoradiograph of this second-generation crystal showed no sign of clusters, and a radiation detector made from it measured a concentration of 6×10^{12} cm^{-3} total carbon (about 95% of the carbon was removed during the process). The physical dimensions of this detector are shown in Fig. 1 (top). It is a 12.8-mm-thick planar crystal with a boron-implanted p^+ contact and a lithium-drifted n^+ contact. The n^+ contact is segmented into a 30-mm-diam central region and an outer guard ring, separated by a 1-mm-wide circular groove. The purpose of the guard ring is to veto events that occur near the edge of the detector. Surface effects on the edge can cause the electric field lines to fringe outward and trap ionization charge at the surface, resulting in incomplete charge collection. In addition, betas from the ^{14}C close to the edge may escape without depositing their

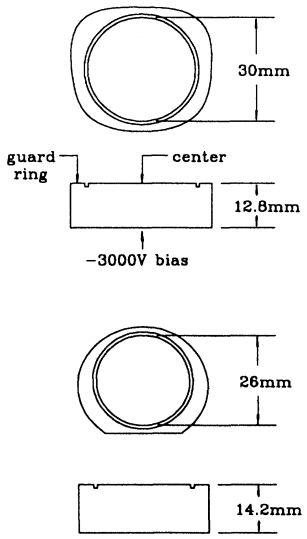

FIG. 1. Dimensions of the ^{14}C-doped germanium detector (top) and the nonradioactive background detector (bottom).

full energy. A small number of betas can still escape near the end contacts without generating a veto, resulting in a small tail in the detector's energy response.

The ^{14}C detector's counting rate was quite low (about 20 sec^{-1}) so environmental background was significant and had to be subtracted. To measure the background, a planar detector with a size and configuration similar to the ^{14}C detector was fabricated from a ^{14}C-free germanium crystal grown using an uncoated silica crucible. It has a thickness of 14.2 mm and a central region 26 mm in diameter. The dimensions of the background detector are shown in Fig. 1 (bottom).

In 1989 the second-generation ^{14}C-doped germanium detector and the nonradioactive background detector were taken out of storage and refurbished at LBL's detector laboratory in order to begin an experiment to search for evidence of massive neutrino emission in the ^{14}C beta spectrum. Initial tests of the detector using calibration gamma sources in the energy range 60–400 keV showed excellent linearity and resolution (1–1.3 keV FWHM). The crystal was installed in a standard gamma-ray detector cryostat with an aluminum end cap. Separate FET integrating preamps for the center region and guard ring were used. The high voltage circuit was configured with a pulser input so that a periodic pulse could be summed with the bias voltage to create a monoenergetic signal in both the center and the guard ring for monitoring gain stability.

There was no practical way to measure the beta response function of the detector using an electron source, so the response function was determined by making the following argument. A low energy gamma ray will interact inside the detector primarily by creating a single photoelectron (and a germanium x ray) which then ionizes the crystal to form an energy signal. This photoelectron is indistinguishable from a beta of the same energy, so its response function should be the same. If the gamma ray interacts instead by Compton scattering and the scattered photon is completely absorbed, a full-energy signal will also be obtained. The observed gamma-ray full-energy peaks can be fit to single-component Gaussians over a wide range of energy, so the photoelectric and Compton-scattered full-energy peak shapes are essentially the same. Therefore the full-energy peak of the beta response function should be well represented by that of the same energy gamma ray. Measurements using calibration sources showed gamma-ray peaks to be Gaussian with widths of 1.0 ± 0.1 keV FWHM in the region 100–160 keV. Figure 2 shows a combined spectrum of ^{241}Am, ^{57}Co, ^{133}Ba, ^{113}Sn, and ^{139}Ce collected in the ^{14}C detector center region with guard ring veto.

The low energy tail of the response will of course be much different for betas than for photons. Only two types of beta events were expected to contribute to the tail: those originating in decays very close (within ~ 100 μm) to the upper and lower surfaces of the crystal that escape without depositing their total energy; and those that cross from the center region to the guard ring (or vice versa) and deposit less than the threshold energy in the guard ring. The size of the tail caused by these events was estimated (assuming uniform distribution of ^{14}C) by

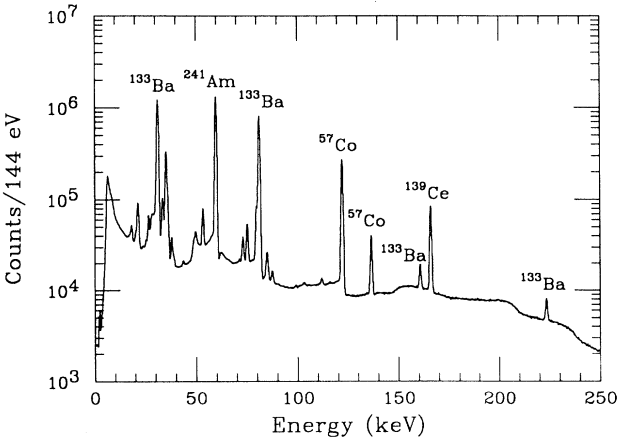

FIG. 2. Combined gamma-ray spectrum of ^{241}Am, ^{57}Co, ^{133}Ba, ^{113}Sn, and ^{139}Ce collected with the ^{14}C detector.

Monte Carlo simulation using the GEANT code [26] and found to be about 0.2% for a 156 keV beta.

III. THE ^{14}C BETA SPECTRUM

Carbon-14 beta decay is an allowed $0^+ \rightarrow 1^+$ Gamow-Teller transition. The beta energy spectrum with a massless neutrino can be written [27]

$$dN(E) = \frac{1}{2\pi^3}\xi C(E)R(E)F(Z,E)pE(Q-E)^2dE. \quad (6)$$

E and p are the beta energy and momentum. The Fermi function $F(Z,E)$ accounts for the final-state interaction between the beta and daughter nucleus; ξ is the energy-independent part of the nuclear matrix element; the spectral shape factor $C(E)$ contains departures from the allowed shape; and $R(E)$ represents radiative corrections. The Fermi function is obtained by evaluating the Dirac wave function of the beta in the Coulomb field of a fixed point source [28]:

$$F(Z,E) = 2\,(\gamma+1)\,\Gamma(2\gamma+1)^{-2}\,(2pR_n)^{2(\gamma-1)} \times \exp\left(\frac{\pi\alpha ZW}{p}\right)|\Gamma(\gamma+i\alpha ZW/p)|^2 \quad (7)$$

with

$$W = E/m_e, \qquad p = \sqrt{W^2-1}, \qquad \gamma = \sqrt{1-(\alpha Z)^2}.$$

R_n is an arbitrary length parameter usually taken to be the nuclear radius. An expansion of $F(Z,E)$ in powers of (αZ), with corrections for nuclear recoil and the finite size of the nucleus, are given in [28]. Screening of the Coulomb field due to atomic electrons can be incorporated by shifting the origin of the Fermi function by V_0:

$$V_0 = N(Z)\alpha^2 Z^{4/3} m_e, \quad (8)$$

where $N(Z)$ is a tabulated function [29]. For the case of

^{14}C, $V_0 = 495$ eV. The Fermi function for ^{14}C, calculated to order $(\alpha Z)^3$ and including nuclear recoil and size and atomic screening corrections, is shown in Fig. 3.

A. Radiative correction

The radiative correction $R(E)$ for beta decay to first order in α has been calculated [30] and is shown in Fig. 3 for the case of ^{14}C. It includes the real inner bremsstrahlung (IB) photons which are emitted in a small fraction of decays and assumes that these photons escape. In the ^{14}C-doped germanium detector most of these photons will be absorbed and their energies summed with the associated beta energies; so the observed radiative correction should be somewhat smaller than the theoretical correction. This effect can be approximately compensated for in the following way. The probability that a beta created with energy W_i emits an IB photon of energy k is given by [31]

$$d\Phi(W_i,k) = \frac{\alpha}{\pi k}\left(\frac{p_f}{p_i}\right)\left[\frac{W_i^2+W_f^2}{W_i p_f}\ln(W_f+p_f)-2\right]dk. \tag{9}$$

W_f and p_f are the energy and momentum of the beta after emitting the photon. The radiative correction due to IB only, when all the photons escape, will be

$$R(E)_{\rm IB} = 1+\left(F(Z,W)\frac{dP_F(W)}{dW}\right)^{-1}\left[\int_W^{W_0} dW'\,F(Z,W)\left(\frac{dP_F(W')}{dW'}\right)\left(\frac{d\Phi(W',k=W'-W)}{dk}\right)\right.$$
$$\left.-\int_1^{W} dW'\,F(Z,W')\left(\frac{dP_F(W)}{dW}\right)\left(\frac{d\Phi(W,k=W-W')}{dk}\right)\right], \tag{10}$$

where $dP_F(W) = pW(W_0-W)^2dW$ is the uncorrected Fermi phase-space factor. The first integral expresses the relative probability that a beta is left with energy W after emitting an IB photon. The second expresses the probability that a beta created with energy W ends up with lower energy due to IB emission. Note that the Fermi function $F(Z,W)$ is applied to the final beta state (after IB emission). If we assume that all IB photons are collected by the ^{14}C detector then the actual radiative correction is

$$R'(E) = 1+R(E)-R(E)_{\rm IB}\ . \tag{11}$$

Of course some of the IB photons will escape the detector, so $R'(E)$ and $R(E)$ should be considered lower and upper limits on the true radiative correction. $R'(E)$ is also shown in Fig. 3.

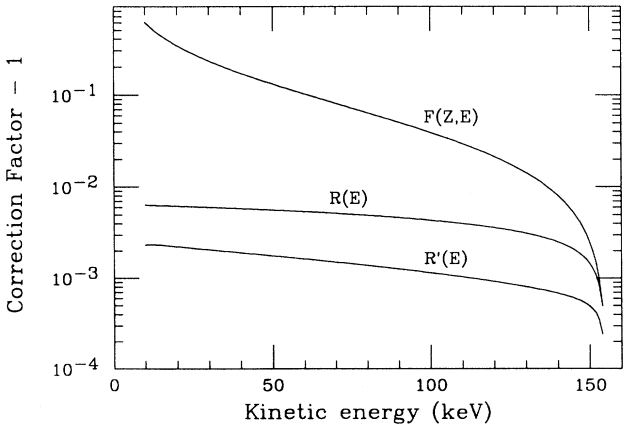

FIG. 3. $F(Z,E)$: ^{14}C Fermi function (Z=7) with corrections for nuclear mass and size; $R(E)$: the first-order radiative correction to ^{14}C beta decay assuming all IB photons escape; $R'(E)$: the radiative correction assuming all IB photons are collected.

B. Induced-current shape factor

The matrix element for ^{14}C decay is expected to have an energy dependence [shape factor $C(E)$] due to the presence of induced weak currents. In a typical beta spectrum this shape factor will be dominated by the interference between the Gamow-Teller (GT) and the weak-magnetism (WM) operators [32]:

$$C(E) \approx 1+\frac{4}{3M}\frac{\langle WM\rangle}{\langle GT\rangle}(E-E_0/2-m_e^2/E)\ , \tag{12}$$

where $\langle GT\rangle$ and $\langle WM\rangle$ are the GT and WM matrix elements; m_e, E, and E_0 are the electron mass, electron energy, and total decay energy; and M is the mass of the nucleus. The WM matrix element can be deduced, assuming conservation of the vector current plus charge independence of the nuclear interactions ($\langle WM\rangle = \langle M1\rangle$), from the strength of the analog M1 electromagnetic transition:

$$\Gamma_{\rm M1} = \frac{1}{6}\alpha E_\gamma^3\frac{\langle M1\rangle^2}{M^2}, \tag{13}$$

and the GT matrix element can be deduced from the β-decay half-life. In the case of ^{14}C the GT matrix element is anomalously small ($\langle GT\rangle \approx 2\times10^{-3}$) and the approximation of Eq. (12) that the shape factor is dominated by the interference of $\langle GT\rangle$ with $\langle WM\rangle$ may not hold. Behrens *et al.* [33] have published complete expressions for the induced-current shape factor, allowing a numerical result if one knows the necessary matrix elements or, equivalently, the wave functions. We use the Behrens *et*

al. expressions to perform a hybrid estimate of the shape factor in ^{14}C. We assume charge independence and use the CVC relation to obtain the WM matrix element from the measured width of the M1 transition of the analog 0^+ level in ^{14}N: $\Gamma_{M1} = (6.7 \pm 0.3) \times 10^{-3}$ eV [34]. We use the WBT shell-model wave functions of Warburton and Brown [35] to calculate other matrix elements (such as the first class induced pseudotensor) except for the GT matrix element. We take the ^{14}C β-decay half-life rather than these wave functions to calculate the GT matrix element because there is a cancellation effect and $\langle GT \rangle$ is very sensitive to uncertainties in the wave functions. We use the full expressions for our calculations and make a linear approximation at the end (deviations from a linear E dependence are negligible). In this way we obtain

$$C(E) = 1 + aE \tag{14}$$

with

$$a = -0.38 \pm 0.04\,\mathrm{MeV}^{-1}\ . \tag{15}$$

This number happens to be equal to an earlier estimate by Calaprice and Holstein [32] in which only the term $\frac{4}{3}\frac{\langle WM \rangle}{\langle GT \rangle}$ was included in Eq. (12). We found that the almost-energy-independent term m_e^2/E, as well as the $E_0/2$ term and others neglected in Eq. (12) significantly affect the value of a due to both the small Q value and the suppressed GT matrix element in ^{14}C decay, and should be included. However these contributions partially cancel, and when we used a more recent value for the width of the M1 transition we arrived coincidentally at the same value for a. The uncertainty in (15) contains the following summed in quadrature: the quoted experimental errors in the ^{14}C half-life and M1 transition width; and the uncertainties in the magnitudes of the additional matrix elements that we calculated using the WBT wave functions (we assumed these uncertainties to be 100%).

The central assumption in the above calculation is that there is no charge-symmetry breaking so that the wave functions of ^{14}C and ^{14}N are the same. Genz *et al.* [36] have recently published phenomenological p^2 wave functions, allowing for charge-symmetry breaking, and used a variety of data to fix their coefficients. They obtained a larger shape parameter for ^{14}C: $a \approx -0.6$ MeV^{-1}. If we similarly relax the constraint of charge symmetry on the wave functions in our calculation, we can obtain values of the shape factor that differ from our estimate in Eq. (15) by up to 50%. This represents an additional uncertainty in our calculation.

In analyzing our experimental spectrum we will treat the shape factor as an additional parameter to be varied in the fits.

IV. THE ORIGINAL EXPERIMENT

In our ^{14}C detector, betas having energies within 17 keV of the end point were collected at a rate of only about 320 per hour. For this reason it was very important to minimize the environmental background counting rate. The experiment was conducted in the Low Background Counting Facility at LBL, which is shielded from the local accelerators by a hillside and covered with 4–5 ft of low-activity concrete. The entire apparatus was surrounded by 10 cm of low-activity lead. The detector can was also enclosed by a graded shield consisting of several mm each of Al, Cu, Cd, and Sn, and a 13-mm-thick brass end plate. In this arrangement the background counting rate was about 2 counts per hour per keV in the energy range 100–160 keV; attributable to natural radioactivity in the cryostat and shielding materials.

Figure 4 shows a schematic diagram of the experiment. Data were accumulated in 1–7 day intervals on a PC-based system using the Ortec MAESTRO data acquisition software. Three Ortec 916 ADC's collected simultaneous spectra: center region singles, guard ring singles, and center region vetoed by the guard ring. Each spectrum contained 4096 channels with 144 eV/channel. A bias of –3000 VDC was supplied to the detector, along with a dual pulser that generated alternating pulses at two energies (10 and 484 keV) with a total rate of 5 Hz. Energy signals were processed using Tennelec 243 amplifiers with 4 μs shaping times, and timing signals were generated using the slow unipolar outputs of Tennelec 248 amplifiers with 0.5 μs shaping times. The guard ring veto threshold was set using an Ortec 551 single channel analyzer (SCA), and the veto logic was made with LBL gate generators and an Ortec 418A universal coincidence module.

Because the ^{14}C betas have such short range in germanium, very few events were expected to produce a

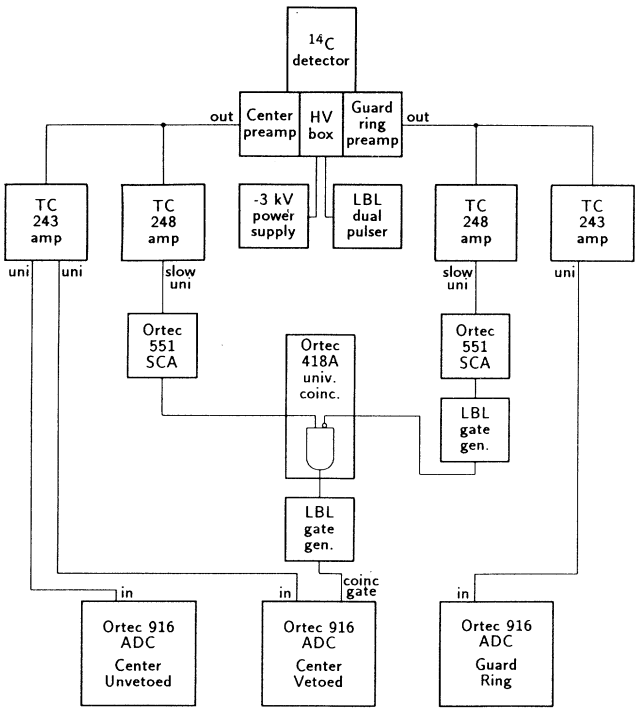

FIG. 4. Schematic diagram of the ^{14}C experiment electronics.

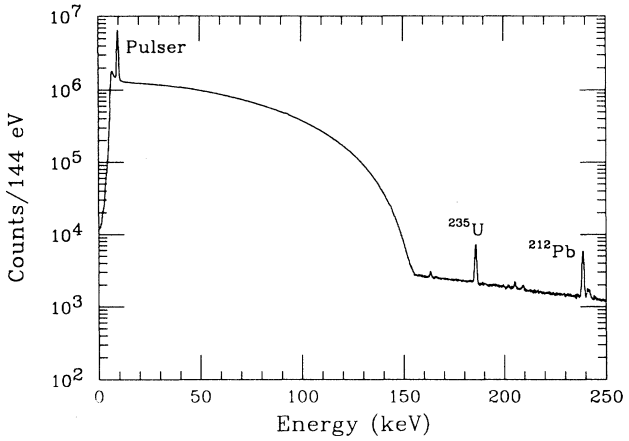

FIG. 5. Total vetoed ^{14}C spectrum collected in 392 days.

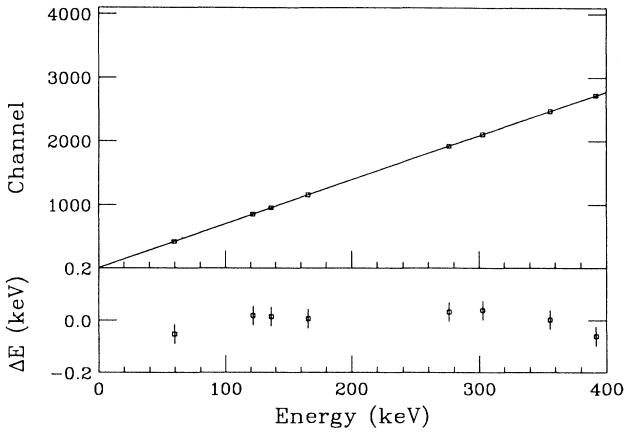

FIG. 7. Gamma-ray calibration of the ^{14}C detector.

true coincidence signal in both the center region and the guard ring. However, capacitive coupling between the center and guard ring electrodes and the ionization region causes a small bipolar image pulse to be generated in one electrode whenever a true signal appears in the other (see [37] for a general discussion of this phenomenon). In order to prevent vetoing a true center region event on the associated bipolar image signal in the guard ring, the guard ring veto lower threshold was set conservatively at 0.47 volts, which is equivalent to a 20 keV energy signal. The upper threshold was set at 4.50 volts, or 183 keV, well above the ^{14}C end point.

A grand total of 392 days of data were collected with the ^{14}C detector. The total vetoed spectrum is shown in Fig. 5. It contains about 3×10^5 counts/keV at 139 keV (the expected kink position for a 17 keV neutrino). An additional 111 days were collected with the background detector installed in the same cryostat. The background spectrum is shown in Fig. 6. All lines in the ^{14}C and background spectra were identified and accounted for as naturally occurring thorium and uranium decay-chain activity.

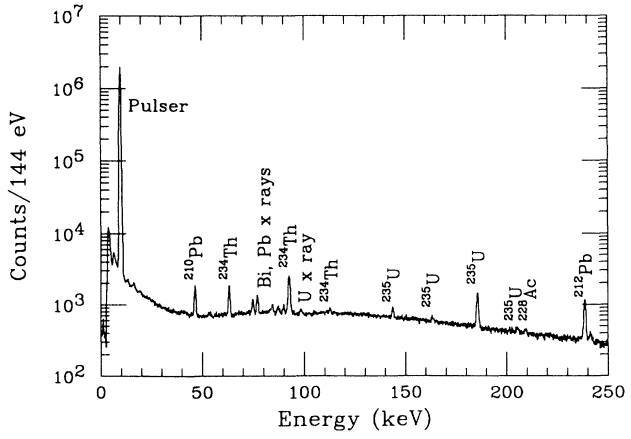

FIG. 6. Total vetoed background spectrum collected in 111 days.

The energy scale of the system was calibrated using gamma-ray sources and the result is shown in Fig. 7. The linearity is superior to that of a typical commercial planar germanium detector. The calibration was monitored over time using the pulser peaks and background lines, and was found to be stable to within ±0.1% over the course of the experiment.

V. INITIAL DATA ANALYSIS

The total vetoed center-region ^{14}C data (392 days) were fit to the theoretical spectrum [Eqs. (3) and (6)] using a nonlinear least-squares fitting routine [38]. The overall amplitude, end-point kinetic energy ($E_0 = Q - m_e$) and neutrino mass parameters (m_2 and $\sin^2\theta$) were allowed to vary freely in the fits. The background detector and ^{14}C detector have different volumes so a live-time background normalization was not appropriate. The background data (111 days) were subtracted with the normalization varied as a free parameter. The spectral shape factor $C(E) = 1 + aE$ was included, with a also varied freely in the fit.

During the fitting process the theoretical spectrum was convoluted with the detector response function, which consisted of a Gaussian full-energy peak and a flat tail with area 0.2%/156 keV (from the GEANT calculation). The presence or absence of this tail had a negligible effect on the outcomes of the fits. Use of a larger tail (up to 4%/156 keV) in the 100–160 keV fits resulted in a smaller value for the shape parameter a and no significant change in the goodness-of-fit or the other parameters. The width of the Gaussian peak was fixed at 1 keV FWHM based on the observed gamma-ray widths. Varying this width by up to ±20%, or including a small energy dependence in the width, did not significantly affect the results.

Table I gives a summary of the fits. Good fits were obtained in the kinetic energy interval 100–160 keV. The best fit is shown in the first column. It calls for a neutrino admixture with mass 16.6 ± 0.6 keV and $\sin^2\theta = 1.25 \pm 0.25\%$, in excellent agreement with the

TABLE I. Results of fitting ^{14}C data (uncertainties are statistical σ).

	Vetoed				Unvetoed
Kinetic energy region fit (keV)	100–160	100–160	100–160	50–160	100–160
Data points	60	60	60	110	60
χ^2	65.0	91.0	65.8	1090.7	60.2
E_0 (keV)	155.78 ± 0.04	155.68	155.78	155.87	155.75
m_2 (keV)	16.6 ± 0.6	16.6[a]	16.6	16.9	16.3
$\sin^2\theta$ (%)	1.25 ± 0.25	0[a]	1.20	2.5	0.77
$(\mathrm{MeV}^{-1})a$	-0.68 ± 0.02	-0.67	-0.67	b	-0.71
Background norm. factor	4.46 ± 0.03	4.50	4.46	4.42	4.58
Rad. correction (Fig. 3.7)	$R'(E)$	$R'(E)$	$R(E)$	$R'(E)$	$R'(E)$

[a]Held fixed during fit.
[b]Not meaningful.

results of Simpson and Hime [2,10]. The second column shows a similar fit where the mixing was fixed at zero. The chi-squared increases by 26 units, a difference of 5σ. The data/fit for this case is shown in Fig. 8. In the upper plot the end-point energy and overall normalization were fit in the region 140–155 keV (above the 17 keV neutrino kink position) and this fit was extrapolated to the lower energies. In the lower plot they are fit using the entire interval (100–160 keV), which gives a truer picture of the statistical significance of the result. In both cases the solid curve represents the expectation with m_2=16.6 keV and $\sin^2\theta$=1.25%.

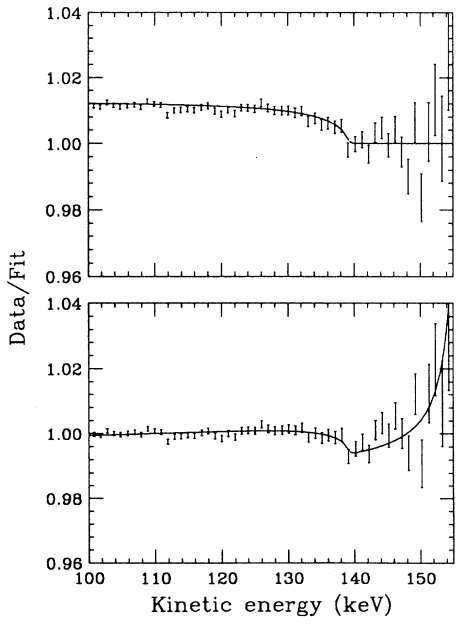

FIG. 8. Data/fit of total vetoed ^{14}C spectrum from 100–160 keV fit to the theoretical spectrum with no massive neutrino. The normalization and end-point energy are fit from 140–155 keV (top) and over the entire interval (bottom). The solid curves show the expected result for $m_2 = 16.6$ keV, $\sin^2\theta = 1.25\%$.

The fits in the first and second columns of Table I both used the radiative correction $R'(E)$ (Fig. 3), which assumes that all IB photons are collected in the detector. The fit shown in the third column used the correction $R(E)$, which assumes that all IB photons escape. This fit was slightly worse, but not by a significant amount. The goodness-of-fit worsened considerably when energies below 100 keV were included in the fits, indicating significant distortion of the spectrum at these energies. For example, the fourth column shows a fit to the energy interval 50–160 keV. The fit was very poor, although the fit values of E_0 and m_2 were consistent with those of the smaller interval. The last column gives the results from a fit to the unvetoed center region data from 100–160 keV. The best-fit value of $\sin^2\theta$ was significantly lower but the results of other parameters were consistent.

The end-point energy E_0 was determined very precisely in the fits and the result was about 700 eV lower than the accepted value [23] of 156.473 keV. The best fit spectral shape parameter a was -0.68 MeV^{-1}.

VI. SYSTEMATIC PROBLEMS AND ADDITIONAL TESTS

The evidence for emission of a 17-keV neutrino in the fits to the ^{14}C data, apparently confirming Simpson's and Hime's results, was very exciting. It helped fuel the debate over its existence. At the time of our original report [11] we had considered and ruled out a number of systematic effects that we thought could mimic a 17-keV neutrino. However there were still some anomalies in the data that were not understood. First of all, the fits were good only in the upper 60 keV of the spectrum and a systematic distortion was increasingly evident as lower energies were included. A good fit should have been obtained over a much larger energy range if the detector was functioning as expected. Another concern was the observed coincidence rate; approximately 9% of the center region signals were vetoed by signals in the guard ring. The guard ring veto threshold at 0.47 V was much higher than the level of the coincident bipolar pulses; and

the expected rate of true coincidences, where the beta deposits energy in both the center and guard ring, was less than 1%.

In order to further study the coincidence signals, a CAMAC-based multiparameter data acquisition system was set up in the Low Background Counting Facility. This allowed the detector's center and guard ring signals to be recorded separately for each event. Six days of ^{14}C data were collected. Figure 9 shows a 2D plot of center vs guard ring energy for coincident events. This picture was quite surprising and difficult to understand. Not only was the coincidence rate very high, a large fraction of the events fell into radial bands with the guard ring energy proportional to the center energy.

In an additional test, the detector was scanned with a highly collimated gamma-ray source. A 500 μCi point source of ^{141}Ce was prepared and placed behind a 500-μm-diameter hole in a $\frac{1}{4}$-in.-thick lead plate. ^{141}Ce has a gamma ray at 145 keV, which is inside the energy range of interest. The attenuation length of this gamma ray in germanium is 1.1 cm, so the entire thickness of the crystal was illuminated in these measurements. Starting at the center of the detector face on the side opposite the groove, the source was moved radially outward in 0.5–1.0-mm increments to the outer edge of the guard ring and a spectrum was collected at each increment. Figure 10 shows a 2D spectrum of center vs guard ring energy at a position of 15.5 mm from the center, directly underneath the groove. The coincidences that sum to 145 keV form a double line. The fainter, straight line contains events where the gamma-ray Compton scattered in the guard ring and the scattered photon was subsequently absorbed in the center, or vice versa. It exhibits the characteristic gap between the Compton photon and electron backscatter edges. This line faded gradually as the source was moved away from the groove. The stronger, slightly curved line was unexpected. It is peaked at one-

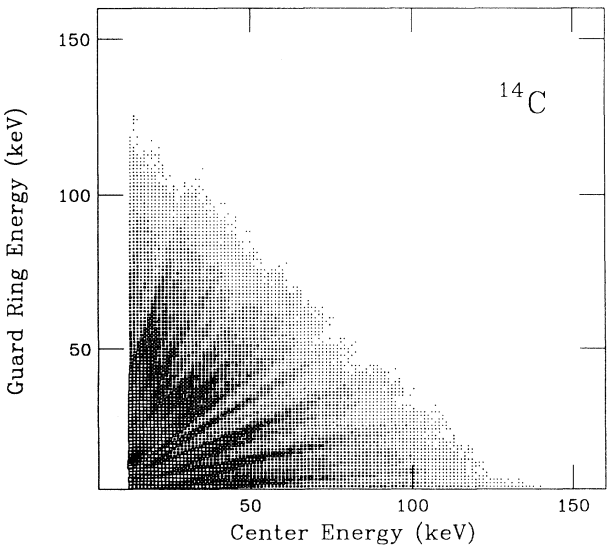

FIG. 9. Center vs guard ring energy for coincident ^{14}C events.

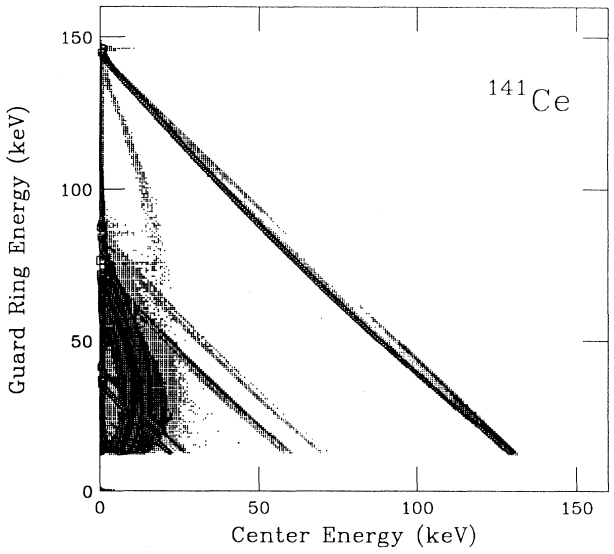

FIG. 10. 2D plot of center vs guard ring energy for coincident ^{141}Ce events. The collimated source was 15.5 mm from the center of the ^{14}C detector (underneath the groove). The effects of charge division under the groove and surface channel trapping of charge are evident (see text).

half of the full energy and it disappeared entirely when the source was moved away from the groove. Its presence indicates that ionization charge was divided between the center and the guard ring when a gamma ray interacted under the groove. The curvature in the coincidence line represents an energy loss, most likely due to a small amount of charge being trapped at the surface of the groove. Charge division under the groove is also seen in the lower energy Pb and Pm x rays.

The "banana"-shaped curves at the left side of Fig. 10 are due to a surface channel that developed at the side surface of the detector. This surface channel caused some of the signal charge created in the guard ring to be trapped at the side surface, resulting in partial signals being induced simultaneously at the center and guard-ring electrodes. This effect is not related to the charge division. Examination of the earlier ^{14}C data showed that the surface channel developed after completion of the initial experiment. This problem was corrected by a surface treatment of the crystal.

The probability of charge division for events under the groove was quantified by comparing the photopeak and tail areas in center and guard ring spectra as the source was scanned across the detector. After accounting for beam divergence, attenuation, and Compton scattering, charge division was observed to occur for about 70% of all interactions under the groove. This explains the high coincidence rate observed in the ^{14}C experiment. The volume under the groove is 13.8% of the volume in the center region. If the ^{14}C is distributed uniformly throughout the crystal, the coincidence rate should be about $(0.7)(0.138)=9.7\%$ due to charge division.

A key piece of information was provided by an earlier experiment in which a position-sensitive, ^{14}C-doped

detector was fashioned from the same second-generation crystal as our detector (see [39] for details). By measuring the time delay between signals at the positive and negative electrodes, the one-dimensional position of each ionization event was obtained. The time spectrum from internal ^{14}C decays contained a number of peaks, each indicating the presence of a carbon cluster, i.e., a large concentration of decays originating from one position. The areas of these peaks showed that the largest clusters contained $1–6 \times 10^{10}$ atoms of total carbon. This result contradicts the earlier autoradiograph that showed no sign of carbon clusters in the ^{14}C-doped crystals of this generation. The autoradiograph technique was not sensitive to clusters of such small size. Our ^{14}C-doped detector should contain similar carbon clusters, since it came from the same original crystal.

The combined effects of carbon clusters and charge division under the groove can explain the radial bands observed in the ^{14}C coincidences (Fig. 9). The ionization charge produced by a beta decay from a cluster located under the groove is split between the center and guard ring. The fraction that goes to each region depends on the exact shape of the electric field lines at that position. The clusters are tiny, so this fraction is constant for all decays originating from the same cluster, and they form a proportional band in the coincidence plot. Each salient band in Fig. 9 was most likely caused by a single cluster under the groove in the ^{14}C detector. The continuum beneath the bands was due to clusters too small to be resolved and/or fully dissolved carbon. Integrating the bands revealed that at least 50% of the total carbon is contained in these clusters. The most prominent bands are each about 1–2 % of the total coincidences. Based on the total counting rate of the crystal these clusters contain about $5–10 \times 10^{10}$ carbon atoms each (including ^{12}C). This is in good agreement with the position sensitive detector test.

What does this mean for the 17-keV neutrino result? In the original measurement, the guard ring veto lower threshold was set at 0.47 V (equivalent to 20 keV energy) in order to prevent vetos from the bipolar image signals. Therefore all charge-divided events under the groove where the guard ring collected less than 20 keV of equivalent charge were not vetoed. They were included along with the "good" ^{14}C events in the center region, and represented an unwanted contamination in the spectrum.

VII. A SECOND MEASUREMENT

A second ^{14}C measurement, using the multiparameter data acquisition system, was conducted in 1993-94 to explore the effect of charge division under the groove on the beta spectral shape. The acquisition system was triggered on center region events with an 8.5 keV threshold. This signal was also used to start an Ortec 457 time-to-amplitude converter (TAC). The TAC was stopped by a guard ring signal with the threshold set as low as possible (< 0.5 keV). Ortec 572 amplifiers were used to produce the center and guard ring energy signals, and the center energy, guard ring energy, and TAC output were recorded for each event. A total of 74 days of ^{14}C data were collected, and an additional 15 days of data were collected with the background crystal in the same configuration. This is about a factor of 5 less data than in the original measurement, so the statistical sensitivity will be less.

Extracting the true center region ^{14}C spectrum would require vetoing all charge-divided events at all energies in the guard ring. However at very low energies (< 5 keV) the guard ring spectrum is dominated by the induced bipolar pulses (discussed in Sec. IV) in coincidence with events in the center. Vetoing on these bipolar pulses would introduce an energy-dependent efficiency for center region events and distort the beta spectrum. Therefore the goal was to veto as many of the charge-division events as possible without vetoing any of the bipolars. Differences in the relative timing of the bipolar and charge-division coincidences between the center and guard ring allowed us to separate most of these signals in the TAC spectrum. We found that the bipolar pulses were all less than 5 keV in the guard ring energy spectrum, and conveniently the charge-division coincidence spectrum dropped off rapidly below 5 keV. The two TAC peaks overlapped by a few percent, so the most effective scheme was to veto all coincident events where the guard ring energy was greater than 5 keV. In this way none of the bipolar signals were vetoed and the only charge division events not vetoed were those that deposited less than 5 keV in the guard ring. The center region ^{14}C spectrum vetoed in this way is shown in Fig. 11, labeled spectrum (1). Also shown in this figure is the center region spectrum vetoed in the same way except with the guard ring veto threshold at 20 keV, labeled spectrum (2). The latter is equivalent to the vetoed spectrum in the original ^{14}C experiment. In addition to the "good" center region ^{14}C events it contains all the charge division events where the guard ring collected between 5 and 20 keV of equivalent charge. These events were inadvertently included in the original experiment because the veto threshold was too high.

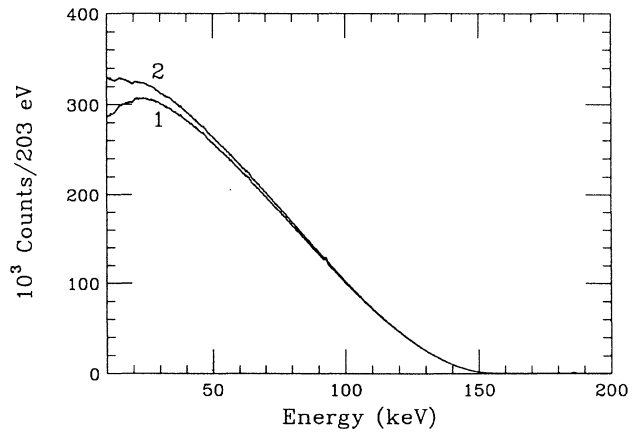

FIG. 11. Vetoed center region ^{14}C spectrum with the guard ring veto threshold at (1) 5 keV and (2) 20 keV.

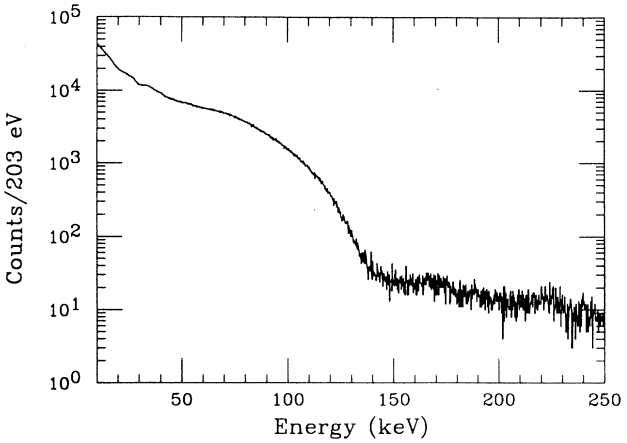

FIG. 12. Center region spectrum in coincidence with guard ring events with energies between 5 and 20 keV [spectrum (2) minus spectrum (1)].

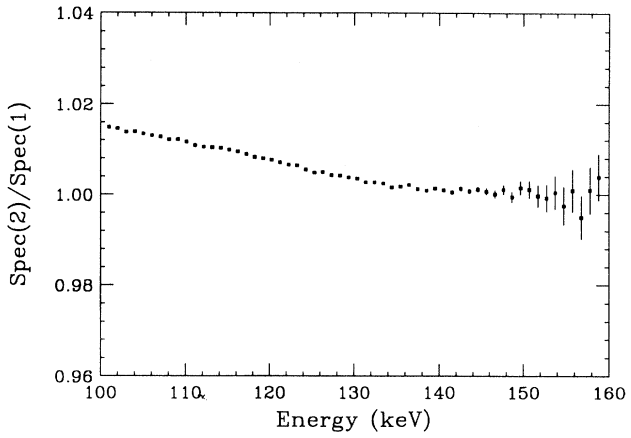

FIG. 13. Vetoed spectrum (2) divided by vetoed spectrum (1), after subtracting background.

What effect did these charge-division events have on the shape of the spectrum? Figure 12 shows the spectrum of these events, the difference between vetoed spectra (2) and (1). It looks roughly like a beta spectrum with an end point at about 140 keV, very close to the 17-keV kink position. Figure 13 shows the ratio of spectrum (2) and spectrum (1). This plot is similar in effect to Fig. 8 (top) in the old data. If the spectrum of events due to charge division under the groove were present with the same shape in the original data, then the two plots would look the same, except for a correction for the different shape parameter a. The ratio would be unity near the end point and deviate at lower energies. The effects are similar in magnitude, and they both begin to rise below about 140 keV. However the shapes are somewhat different; the older data show a more sudden jump at the kink position, more akin to the threshold expected for a massive neutrino admixture. Also, the effect in Fig. 13 should be higher (about 1.025 at 100 keV) to simultaneously explain both the 17-keV neutrino and the higher shape parameter a in the older data.

The new data were fit to the theoretical beta spectrum in a number of different ways. The results of fitting spectrum (1) are summarized in Table II. Good fits were obtained in the energy region 100–160 keV. The previous result of a 16.6-keV neutrino with $\sin^2\theta = 1.25\%$ is now excluded at 80% C.L. ($\Delta\chi^2 = 2$). The shape parameter a is now -0.45 MeV^{-1}, slightly larger than the calculated value of -0.38 ± 0.04 MeV^{-1} (Sec. III B). Fits to a wide energy region, 50–160 keV, are still somewhat poor but greatly improved from the original experiment. The best-fit values of the shape parameter and end point energy are lower in the wide region, presumably due to the residual distortion. The 1.25%, 16.6-keV neutrino is rejected in this energy region as well.

Spectrum (2), which should be equivalent to the vetoed spectrum in the original experiment, was also fit. The result of this fit is also shown in Table II. The shape parameter a and end-point energies are consistent with those of the original vetoed spectrum, but the preference for a 17-keV neutrino is gone. The 1.25%, 16.6-keV neutrino is now excluded at 90% C.L. ($\Delta\chi^2 = 3$). Apparently something changed during the 2 years that separate the two measurements. This change is most likely related to the difference in shape seen in plots of the recent measurement of the 20-keV veto effect (Fig. 13) and the original 17-keV neutrino effect [Fig. 8 (top)]. What could have caused this? We have noticed that the positions of the

TABLE II. New ^{14}C fit results (uncertainties are statistical σ). The radiative correction $R'(E)$ was used for all fits.

	Spectrum (1)				Spectrum (2)
Kinetic energy region fit (keV)	100–160	100–160	50–160	50–160	100–160
Data points	60	60	110	110	60
χ^2	66.8	68.8	173.1	185.9	71.0
E_0 (keV)	155.67 ± 0.08	155.75	155.46	155.55	155.66 ± 0.07
m_2 (keV)	16.6[a]	16.6[a]	0[a]	16.6[a]	16.6[a]
$\sin^2\theta$ (%)	0.4 ± 0.6	1.25[a]	0[a]	1.25[a]	0.1 ± 0.6
(MeV^{-1})a	-0.45 ± 0.04	-0.46	-0.32	-0.34	-0.63 ± 0.05
Background norm. factor	6.81 ± 0.13	6.88	7.19	7.13	6.77 ± 0.14

[a]Held fixed during fit.

radial bands in 2D center/guard ring coincidence plots have changed over several years' time. Figure 14 shows a comparison of 6 days of data collected in May 1992 (simply a magnified view of Fig. 9) and 7 days of data collected in December 1993. It appears that the coincidence bands rotated relative to each other. The detector was removed several times from the cryostat during this time period and its surfaces were chemically treated, but it was never heated above room temperature so the carbon clusters cannot have moved. However we know that the electric field lines in the guard ring are very sensitive to the chemical condition of the surface at the edges of the crystal. This was evidenced by the "banana"-shaped surface channel coincidences present when the ^{141}Ce tests were done (see Fig. 10 and the discussion in Sec. VI). It is reasonable to expect that changing the shape of the electric field in the guard ring will affect the shape of the field lines under the groove. This will in turn change the proportion of charge split between the center and guard ring for a particular carbon cluster under the groove, causing the corresponding coincidence band to rotate. This may explain the changes we have observed in the ^{14}C data.

We emphasize that the quoted confidence levels excluding a 17-keV neutrino reflect only the statistical uncertainties in the fits and ignore any systematic uncertainties. They are intended only as a means of comparing different data and analyses within this experiment. The existence of a 17-keV neutrino has been excluded more conclusively by other experiments (e.g. [14–16]).

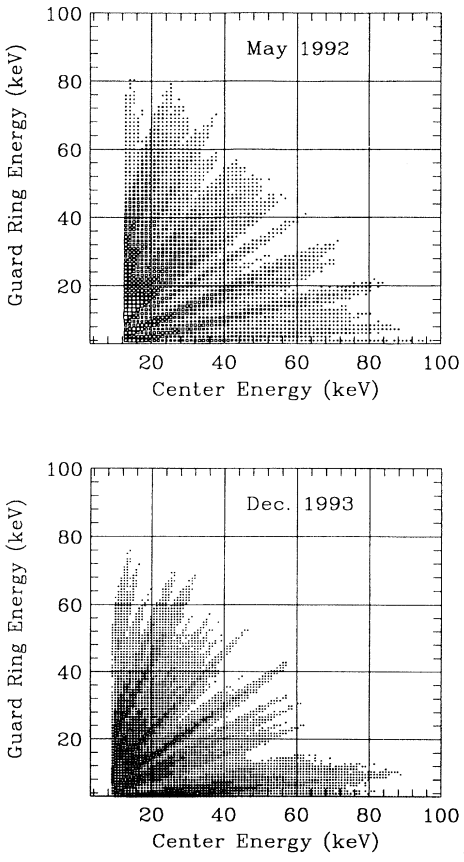

FIG. 14. Center vs guard ring 2D coincidence plots for data taken in May 1992 (top) and December 1993 (bottom).

VIII. THE END-POINT ENERGY

The observed end-point energy in all of the ^{14}C spectra (old and new) is significantly less than the accepted value of 156.473 keV [23], which is strongly weighted by the 1974 mass spectrometer measurement of Smith and Wapstra [40]: Q=156.476 ± 0.005 keV. The end-point energy is equal to Q plus the binding energy of the $2p^{\frac{1}{2}}$ electron in ^{14}N (−11.8 eV [41]). The gamma-ray calibration of the ^{14}C-doped detector was excellent (see Fig. 7) in the vicinity of the end point and should be correct for events fully contained in the center region. Of course, we must account for some systematic effects in the data that could affect the end-point energy determination.

By differentiating Eq. (6) with respect to Q we note that the fractional change in the shape of the beta spectrum corresponding to a small change in Q is proportional to $\Delta Q/(Q-E)$. Consequently, the spectral shape near the end point is much more sensitive to Q than the shape at lower energy. On the other hand, the relative statistical errors in the data are proportional to $[pE(Q-E)^2]^{-\frac{1}{2}}$. Therefore the sensitivity to Q in the chi-squared goes as $\sqrt{pE}$ and so spectral distortions at lower energies have a significant effect on determining the end point energy in a least-squares fit. We can reduce the influence of low energy shape distortions by restricting the analysis to energies close to the end point, where we obtain good fits. To this end, ^{14}C spectrum (1) was fit in the region 120–160 keV. The best fit gave E_0=155.79 ± 0.07 keV with χ^2=35.8/36 d.o.f. The data divided by best fit are shown in Fig. 15 (top). Now, this choice of fit region was to some extent arbitrary and we expect that, given some distortion of the spectrum, the best-fit end-point energy will vary systematically with the region fit. The size of this effect was estimated by performing a number of fits with different starting energies (e.g., 110–160 keV, 130–160 keV). We found that E_0 varied over a range of 120 eV, which we take as the systematic uncertainty in E_0 due to distortion in the spectral shape. In addition to this we expect that the end-point energy determination will be affected by systematics in the vicinity of the end point, where there are two problems of concern.

First, betas originating in carbon clusters will lose some energy. This can affect the shape of the spectrum, but close to the end point it mainly causes a downshift of the observed spectrum by the average energy loss. The ^{14}C coincidence bands (Fig. 9) and the position-sensitive detector results [39] both indicate a maximum cluster size of about 10^{11} atoms. A 150-keV beta starting from the center of a spherical cluster of this size will lose about 400 eV in the carbon [24]. If the ^{14}C is uniformly distributed inside this cluster, and the betas are emitted in random directions, then the average energy loss will be 3/4 of this, or 300 eV. The average cluster size is much

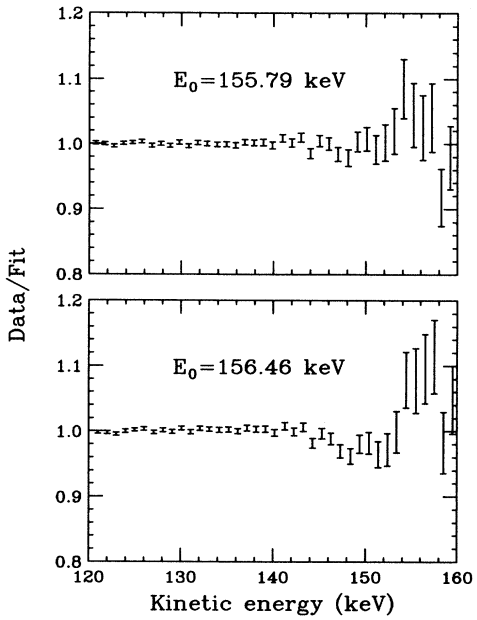

FIG. 15. Data/fit from fits to ^{14}C spectrum (1) in the energy range 120–160 keV, with the end-point energy varied in the fit (top) and fixed at 156.46 keV (bottom). The data in the lower plot are shifted up in energy by 0.3 keV (see text).

smaller than 10^{11} atoms, so the average energy loss in all the carbon clusters will be much less. However, since the size distribution of the clusters is not well known, we conservatively estimate the average energy loss (near the end point) to lie in the range 150 ± 150 eV.

Second, the background subtraction near the end point is imperfect. The geometry of the background detector is different from that of the ^{14}C-doped detector, so the peak area ratios of background lines and the shape of the background continuum are not quite the same in the ^{14}C and background spectra. This problem can be seen in Fig. 15 (top) as a slight distortion above about 140 keV. The effect of this on the end-point energy was estimated by fitting the background in the ^{14}C spectrum in various regions above and below the end point with polynomial functions and subtracting it. In each case the best fit end-point energy was lower than that obtained using the background detector spectrum. The largest change was 80 eV, so we take this as the systematic uncertainty in the end-point energy caused by the background subtraction.

With these systematic errors summed in quadrature we have our result: E_0=155.94 ±0.07 (stat) ±0.21 (sys) keV. We stress that while the quoted statistical errror is 1σ, the systematic error is much more conservative and should not be regarded as 1σ. We performed another fit of the same data in a similar way except with E_0 fixed at the Smith and Wapstra value of 156.46 keV. To accommodate the energy loss in the carbon clusters in the most conservative way, the data were shifted up in energy by 300 eV (the maximum estimated average loss) prior to this fit. We obtained χ^2=69.2/37N_{DF} The data/fit plot for this result are shown in Fig. 15 (bottom). It is apparent from this plot that the disagreement occurs near the end point and not in the shape at lower energies.

IX. CONCLUSIONS

Much progress has been made in understanding the behavior of the ^{14}C-doped germanium detector since the first experiment in 1991. The demonstrated presence of charge division under the groove and carbon clusters invalidates the original analysis that showed evidence of a 17-keV neutrino admixture in the spectrum [11] and we retract that result. We were unable to reproduce the heavy neutrino signal in the second measurement, so we cannot be certain of its cause. However there is strong circumstantial evidence that it was due to contamination of the beta spectrum by decays under the groove where the charge was split and the guard ring collected less than 20 keV of equivalent charge. This contamination spectrum has an end point very close to the kink position (about 140 keV, see Fig. 12) and about the correct magnitude (1.5%, see Fig. 13). There is also some evidence that the shape of this effect changed over time. In any case, the most recent data no longer support the presence of 17-keV neutrino emission in the ^{14}C beta spectrum.

Even with the new data we are unable to obtain a good fit to the theoretical spectrum over a wide energy range. The experiment remains limited by systematic problems. The background subtraction is imperfect. Low energy charge-division signals and the bipolar image signals cannot be completely discriminated in the guard ring. Finally, energy loss in the carbon clusters probably causes some distortion of the spectrum. It is possible that theoretical uncertainties in forbidden corrections to the spectral shape factor $C(E)$ also contribute to our difficulties in fitting the data. The best-fit value for the linear shape parameter a varies significantly with the region fit, so we cannot confidently claim a result for it. Still, it is encouraging that in fits to the high energy region 100–160 keV we obtain a value for a that is close to our calculated value.

Finally, in spite of the various problems with this experiment, we believe that our determination of the Q value is correct. We feel there is a significant problem in the ^{14}C Q value and we hope that this will be resolved by future experiments.

ACKNOWLEDGMENTS

We wish to thank C.P. Cork, F.S. Goulding, D.A. Landis, N.W. Madden, R.J. McDonald, and A.R. Smith for their support and assistance in various aspects of the experiment. This work was supported by the Director, Office of Energy Research, Division of Nuclear Physics of the Office of High Energy and Nuclear Physics of the U.S. Department of Energy under Contracts Nos. DE-AC03-76SF00098 and DE-FG05-87ER40314. M.T.F.C. was supported in part by Fundação de Amparo à Pesquisa do Estado de São Paulo, FAPESP, São Paulo, Brazil.

[1] F. Boehm and P. Vogel, *Physics of Massive Neutrinos,* 2nd edition (Cambridge University Press, Cambridge, England, 1991), p. 70.
[2] J.J. Simpson, Phys. Rev. Lett. **54**, 1891 (1985).
[3] T. Altzitzoglou, F. Calaprice, M. Dewey, M. Lowry, L. Piilonen, J. Brorson, S. Hagen, and F. Loeser, Phys. Rev. Lett. **55**, 799 (1985).
[4] A. Apalokov *et al.*, JETP Lett. **42**, 289 (1985).
[5] J. Markey and F. Boehm, Phys. Rev. C **32**, 2215 (1985).
[6] D.W. Hetherington, R.L. Graham, M.A. Lone, J.S. Geiger, and G.E. Lee-Whiting, Phys. Rev. C **36**, 1504 (1987).
[7] V.M. Datar, C.V.K. Baba, S.K. Bhattacherjee, C.R. Bhuinya, and A. Roy, Nature (London) **318**, 547 (1985).
[8] T. Ohi, M. Nakajima, H. Tamura, T. Matsuzaki, T. Yamakazi, O. Hashimoto, and R.S. Hayano, Phys. Lett. **160B**, 322 (1985).
[9] ISOLDE Collaboration, M.J.G. Borge, A. De Rújula, P.G. Hansen, B. Jonson, G. Nyman, H.L. Ravn, and K. Riisager, Phys. Scr. **34**, 591 (1986).
[10] J.J. Simpson and A. Hime, Phys. Rev. D **39**, 1825 (1989); A. Hime and J.J. Simpson, *ibid.* **39**, 1837 (1989).
[11] B. Sur, E.B. Norman, K.T. Lesko, M.M. Hindi, R.M. Larimer, P.N. Luke, W.L. Hansen, and E.E. Haller, Phys. Rev. Lett. **66**, 2444 (1991).
[12] A. Hime and N.A. Jelley, Phys. Lett. B **257**, 441 (1991); A. Hime, D. Phil. Thesis, Oxford 1991 (unpublished).
[13] I. Žlimen, A. Ljubičić, S. Kaučić, and B.A. Logan, Phys. Rev. Lett. **67**, 560 (1991).
[14] H. Kawakami *et al.*, Phys. Lett. B **287**, 45 (1992); T. Ohshima *et al.*, Phys. Rev. D **47**, 4840 (1993).
[15] J.L. Mortara, I. Ahmad, K.P. Coulter, S.J. Freedman, B.K. Fujikawa, J.P. Greene, J.P. Schiffer, W.H. Trzaska, and A.R. Zeuli, Phys. Rev. Lett. **70**, 394 (1993).
[16] F.E. Wietfeldt, Y.D. Chan, M.T.F. da Cruz, A. García, R.M. Larimer, K.T. Lesko, E.B. Norman, R.G. Stokstad, and I. Žlimen, Phys. Rev. Lett. **70**, 1759 (1993).
[17] M. Chen, D.A. Imel, T.J. Radcliffe, H. Henrikson, and F. Boehm, Phys. Rev. Lett. **69**, 3151 (1992).
[18] G.E. Berman, M.L. Pitt, F.P. Calaprice, and M.M. Lowry, Phys. Rev. C **48**, R1 (1993).
[19] D.E. DiGregorio, S. Gil, H. Huck, E.R. Batista, A.M.J. Ferrero, and A.O. Gattone, Phys. Rev. C **47**, 2916 (1993).
[20] M. Bahran and G. Kalbfleisch, Phys. Lett. B **291**, 336 (1992); G. Kalbfleisch and M. Bahran, *ibid.* **303**, 355 (1993).
[21] H. Abele, G. Helm, U. Kania, C. Schmidt, J. Last, and D. Dubbers, Phys. Lett. B **316**, 26 (1993).
[22] M.M. Hindi, R.L. Kozub, and S.J. Robinson, Phys. Rev. C **49**, 3289 (1994).
[23] E. Browne and R.B. Firestone, *Table of Radioactive Isotopes* (Wiley, New York, 1986).
[24] L. Pages, E. Bertel, H. Joffre, and L. Sklavenitis, At. Data **4**, 1 (1972).
[25] E.E. Haller, W.L. Hansen, P. Luke, R. McMurray, and B. Jarrett, IEEE Trans. Nucl. Sci. **29**, 745 (1982).
[26] R. Brun *et al.*, GEANT3, CERN, DD/EE/84-1 (1987).
[27] M. Morita, *Beta Decay and Muon Capture* (Benjamin, Reading, Mass., 1973) p. 33.
[28] D.H. Wilkinson, Nucl. Instrum. Methods Phys. Res. Sect. A **275**, 378 (1989).
[29] H. Behrens and W. Bühring, *Electron Radial Wave Functions and Nuclear Beta Decay* (Clarendon Press, Oxford, England, 1982), pp. 146 and 147.
[30] A. Sirlin, Phys. Rev. **164**, 1767 (1967).
[31] J.K. Knipp and G.E. Uhlenbeck, Physica **3**, 425 (1936).
[32] F.P. Calaprice and B.R. Holstein, Nucl. Phys. **273**, 301 (1976).
[33] H. Behrens, H. Genz, M. Conze, H. Feldmeir, W. Stock, and A. Richter, Ann. Phys. (N.Y.) **115**, 276 (1978).
[34] F. Ajzenberg-Selove, Nucl. Phys. **A523**, 1 (1991).
[35] E.K. Warburton and B.A. Brown, Phys. Rev. C **46**, 923 (1992).
[36] H. Genz, G. Kühner, A. Richter, and H. Behrens, Z. Phys. A **341**, 9 (1991).
[37] V. Radeka, Annu. Rev. Nucl. Part. Sci. **38**, 217 (1988).
[38] STEPIT, written by J.P. Chandler, University of Indiana, Bloomington, IN.
[39] P.N. Luke and E.E. Haller, J. Appl. Phys. **59**, 3734 (1986).
[40] L.G. Smith and A.H. Wapstra, Phys. Rev. C **11**, 1392 (1974).
[41] K.-N. Huang, M. Aoyagi, M.-H. Chen, and B. Crasemann, At. Data Nucl. Data **18**, 243 (1976).